SCIENCE CHINA
Chemistry

•ARTICLES•

December 2021 Vol.64 No.12: 2161–2168
https://doi.org/10.1007/s11426-021-1121-y

High-efficiency organic solar cells enabled by an alcohol-washable solid additive

Yuanpeng Xie[1], Hwa Sook Ryu[2], Lili Han[3], Yunhao Cai[1*], Xiaopeng Duan[1], Donghui Wei[3], Han Young Woo[2*] & Yanming Sun[1*]

[1]*School of Chemistry, Beihang University, Beijing 100191, China;*
[2]*Department of Chemistry, College of Science, KU-KIST Graduate School of Converging Science and Technology, Korea University, Seoul 136-713, Korea;*
[3]*College of Chemistry and Molecular Engineering, Zhengzhou University, Zhengzhou 450001, China*

Received August 12, 2021; accepted September 8, 2021; published online October 18, 2021

The solvent additive strategy has been widely utilized to boost the power conversion efficiency (PCE) of organic solar cells (OSCs). However, the residual solvent additive in the active layer tends to induce a gradual morphology degradation and further influences the long-term stability of OSCs. Here, a solid additive, 1,4-diiodobenzene (DIB), was introduced to fabricate efficient OSCs. We found that the treatment of DIB can lead to optimized morphology to form a bicontinuous network with intensified intermolecular packing in the donor and acceptor phases. Notably, DIB can be easily removed from the active layer *via* a simple alcohol washing process and no further post-thermal annealing is needed, which is desirable for large-scale manufacturing of OSCs. As a result, high efficiencies of 17.47% for PM6:Y6 and 18.13% (certified as 17.7%) for PM6:BTP-eC9 binary OSCs are achieved, which are among the highest efficiencies reported for binary OSCs thus far. Moreover, OSCs fabricated with DIB also exhibit superior stability compared with the as-cast and traditional solvent additive processed devices. Additionally, DIB was successfully applied in different active layers, manifesting its general applicability. This work provides a feasible approach to enhance both the efficiency and stability of OSCs.

organic solar cells, solid additive, alcohol washing process, efficiency, stability

Citation: Xie Y, Ryu HS, Han L, Cai Y, Duan X, Wei D, Woo HY, Sun Y. High-efficiency organic solar cells enabled by an alcohol-washable solid additive. *Sci China Chem*, 2021, 64: 2161–2168, https://doi.org/10.1007/s11426-021-1121-y

1 Introduction

The rapid progress in the development of non-fullerene acceptors (NFAs) has led to significant improvements in organic solar cells (OSCs) [1–5]. At present, the best-performing OSCs yield power conversion efficiencies (PCEs) over 18% [6–10]. For the commercialization of OSCs, high efficiency, long-term device stability, low cost, and large-scale manufacturing are equally important [11–15]. It was established that the formation of optimal bulk-heterojunction (BHJ) morphology with bicontinuous network in OSCs is the prerequisite for efficient exciton dissociation and charge transport [16–21]. To acquire an optimal morphology, the solvent additives, such as 1,8-diiodooctane (DIO), 1-chloronaphthalene (CN), are widely used in the fabrication of OSCs. Since the solubilities of the donor and the acceptor materials in the solvent additive are different, the molecular aggregation and phase separation in the active layer can be well manipulated [22–27].

Although the use of solvent additives has gained great success in boosting the efficiency of OSCs, there still exists

*Corresponding authors (email: caiyunhao@buaa.edu.cn; hywoo@korea.ac.kr; sunym@buaa.edu.cn)

several challenges for their application in the large-scale manufacturing of OSCs. The solvent additives usually remain in the active layer due to their high boiling point [28], and the residual solvent additives tend to cause morphology degradation and thus influence the long-term stability of OSCs [29–32]. In addition, some of the solvent additives are expensive, the high cost is unsuitable for the commercialization of OSCs. Alternatively, the solid additive is another promising candidate for BHJ morphology control [33,34]. It has been reported that the molecular crystalline ordering can be manipulated through intermolecular interactions between the solid additive and the donor/acceptor materials, and thereby improves the device performance. However, for the use of most solvent/solid additives, post-thermal annealing (TA) is usually needed to further optimize the phase separation and BHJ morphology [35–37]. Especially for the solid additives, the TA treatment is essential in the removal of them. In some cases, the annealing temperature even reaches 150 °C [38–41], which is unfavorable for large area roll-to-roll manufacture.

Herein, DIB was introduced as a solid additive to boost the performance and stability of OSCs. It was found that DIB can grow into microcrystal, which improves polymer interchain packing and induces non-fullerene acceptor aggregation. Moreover, the DIB treatment can afford an optimal bicontinuous network morphology, which could lead to a decent fill factor (FF). Of note is that, for the processing of DIB, neither thermal annealing nor solvent annealing is needed. It can be removed just *via* a simple alcohol washing process. Such treatment is cost-effective, meeting the fundamental requirement for the large-scale manufacturing of OSCs. As a result, impressive PCEs of 17.47% for PM6:Y6 and 18.13% for PM6:BTP-eC9 (certified as 17.7%) binary OSCs processed with DIB are achieved. In addition, OSCs based on PM6:N3, PTB7-Th:IEICO-4F, and P3:Y6 blends were also fabricated. In these systems, superior PCEs were obtained in DIB processed OSCs compared with the devices with traditional solvent additives, testifying the universal applicability of DIB in the fabrication of high-efficiency OSCs. Moreover, the OSCs processed with DIB also exhibited excellent long-term storage stability and photostability.

2 Results and discussion

The chemical structures of DIB, polymer donors, and non-fullerene acceptors used in this article are shown in Figure 1a. DIB is a yellow flake crystal with a melting point of ~132 °C. It can be well dissolved in chloroform (CF) and different alcohols. As shown in Figure S1 (Supporting information online), DIB has good solubility of ~160 mg mL^{-1} in CF, ~20 mg mL^{-1} in methanol (MeOH), and ~16 mg mL^{-1} in isopropanol. These features enable us to develop an alcohol-washing strategy to remove DIB after the preparation of photoactive films. Figure 1b shows a schematic diagram of the alcohol-washing procedures. In detail, the blends of photoactive materials with different DIB contents were dissolved in CF solvent and subsequently spin cast on the top of the substrate. Then, we simply soaked the film into methanol for 5 s to remove the DIB solid additive. In this article, we mainly took the classic PM6:Y6 system as a representative to study the effect of DIB. Figure 1c, d present the UV-vis absorption spectra of neat PM6 and Y6 films with different DIB contents. DIB has negligible absorption in the wavelength range of 300–900 nm (Figure S2). Interestingly, the addition of 0–200 wt% DIB into neat PM6 and Y6 films leads to a red-shift in the absorption spectra. In addition, the maximum absorption coefficients of PM6:Y6 film with 200 wt% DIB were measured to be 5.04×10^4 cm^{-1} at 626 nm and 5.41×10^4 cm^{-1} at 820 nm, respectively, higher than those of as-cast PM6:Y6 film (4.65×10^4 cm^{-1} at 623 nm and 5.07×10^4 cm^{-1} at 801 nm) (Figure S3). This result suggests that DIB processing may increase the intermolecular packing of both PM6 and Y6, which will be discussed in the grazing incident wide-angle X-ray scattering (GIWAXS) section.

To evaluate the effect of DIB on the photovoltaic performance of PM6:Y6 blend, OSCs were fabricated with a conventional device structure of indium tin oxide (ITO)/poly(3,4-ethylenedioxythiophene):poly(styrenesulfonic acid) (PEDOT:PSS)/active layer/poly[(9,9-bis(3′-(*N*,*N*-dimethylamino)propyl)-2,7-fluorene)-alt-5,5′-bis(2,2′-thiophene)-2,6-naphthalene-1,4,5,8-tetracaboxylic-*N*,*N*′-di(2-ethylhexyl) imide] (PNDIT-F3N)/silver (Ag). The current density-voltage (*J*-*V*) curves of OSCs processed with different DIB contents (from 0 to 300 wt%) are shown in Figure S4, and the device parameters are summarized in Table S1 (Supporting information online). As-cast PM6:Y6 OSCs without processing any additives and post treatments exhibited a maximum PCE of 16.46%, with a short-circuit current density (J_{sc}) of 26.01 mA cm^{-2}, an open-circuit voltage (V_{oc}) of 0.853 V, and a FF of 74.2%. When DIB was added into the PM6:Y6 blend, V_{oc} decreases whereas J_{sc} and FF increase simultaneously. When the DIB content reaches 200 wt%, PM6:Y6 devices shows the best PCE of 17.47%, with a high J_{sc} of 26.62 mA cm^{-2}, a high FF of 78.7% and a V_{oc} of 0.834 V. In stark contrast, PM6:Y6 OSCs processed with CN additive and TA treatment produces a PCE of 17.02%, with a J_{sc} of 26.44 mA cm^{-2}, a FF of 77.0% and a V_{oc} of 0.836 V (Figure 1e and Table 1). The results suggest that the DIB treatment can simultaneously increase the J_{sc} and FF of OSCs. The corresponding external quantum efficiency (EQE) spectra of OSCs fabricated under different conditions are shown in Figure 1f. The integrated current densities are 25.67, 26.11 and 26.24 mA cm^{-2} for the as-cast, CN- and DIB-processed OSCs, respectively, which are well consistent

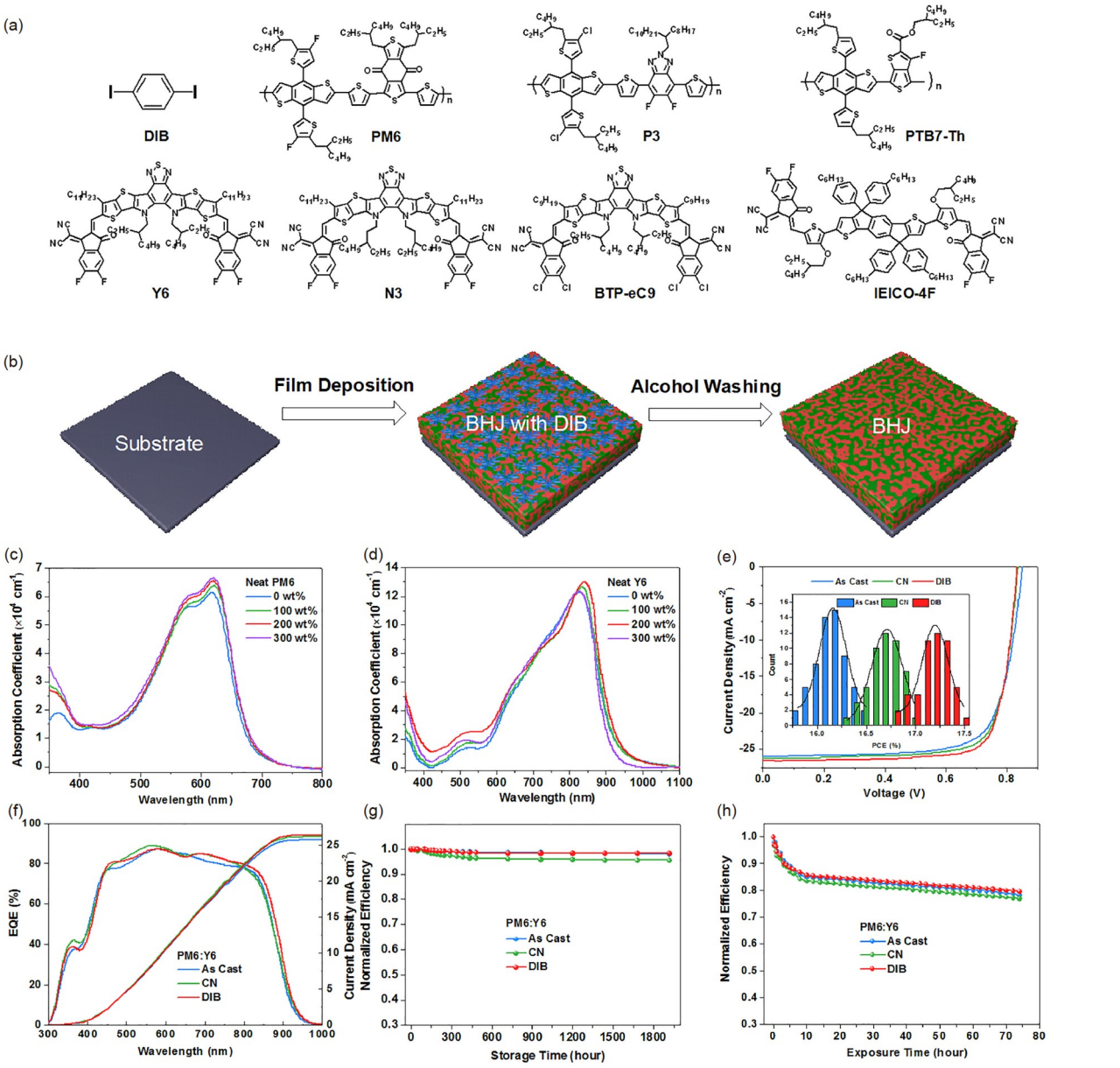

Figure 1 Chemical structures and photoelectric property. (a) Chemical structure of solid additive and photovoltaic materials used in this work. (b) Schematic illustration of fabrication procedure of OSCs using an alcohol-washable solid additive. Absorption spectra of PM6 films (c) and Y6 films (d) processed with different DIB contents. (e) *J-V* characteristics and the histogram of the efficiency measurements of as-cast, CN- and DIB-processed OSCs, and (f) the corresponding EQE spectra and integrated current densities. (g) Long-term stability of as-cast, CN- and DIB-processed OSCs stored in a nitrogen-filled glovebox. (h) Photostability of as-cast, CN- and DIB-processed OSCs under the illumination of an AM 1.5 G solar simulator, 100 mW cm^{-2} (color online).

with the values achieved from the *J-V* measurements.

Subsequently, the general applicability of DIB was verified by introducing it into different active layers, including PM6:N3, PM6:BTP-eC9, PTB7-Th:IEICO-4F, and P3:Y6. The representative *J-V* curves and the corresponding EQE spectra are shown in Figures S5 and S6, and the detailed photovoltaic parameters are summarized in Table 1. The DIB-processed OSCs exhibited superior photovoltaic performance with higher PCEs and FFs compared with those of the as cast and CN- or DIO-processed devices. As a result, a PCE of 17.25% with a FF of over 79.1% is obtained for PM6:N3 device. In particular, PM6:BTP-eC9 device yields an impressively high FF of 79.8% and a PCE of 18.13% (certified as 17.7%, Figure S7), representing one of the highest PCEs reported for binary OSCs so far.

Furthermore, the long-term storage stability and photostability of OSCs processing *via* different methods were investigated. As illustrated in Figure 1g, the DIB-processed OSC with encapsulation maintains 98.2% of its initial efficiency after 1,920 h storage in a nitrogen-filled glovebox, revealing higher storage stability relative to 98.0% of as-cast and 95.4% of the CN-processed devices. As shown in Figure

Table 1 Summary of the photovoltaic parameters of OSCs

Active layer	Additives[a)]	J_{sc} (mA cm^{-2})	V_{oc} (V)	FF (%)	PCE [b)] (%)
PM6:Y6	As Cast	25.54±0.30	0.848±0.005	74.5±0.5	16.14±0.21(16.46)
	CN (71 wt%)	26.30±0.27	0.833±0.003	76.0±1.0	16.70±0.28(17.02)
	DIB (200 wt%)	26.30±0.20	0.832±0.003	78.9±0.4	17.25±0.14(17.47)
PM6:N3	As Cast	25.21±0.20	0.851±0.003	70.5±0.5	15.13±0.12(15.25)
	CN (71 wt%)	26.42±0.27	0.818±0.003	75.9±0.5	16.39±0.26(16.63)
	DIB (200 wt%)	26.34±0.16	0.827±0.003	78.5±0.8	17.11±0.13(17.25)
PM6:BTP-eC9	As Cast	25.40±0.20	0.866±0.002	72.2±0.4	15.88±0.17(16.07)
	DIO (110 wt%)	26.84±0.20	0.833±0.004	78.3±0.8	17.52±0.25(17.82)
	DIB (200 wt%)	26.44±0.18	0.856±0.001	79.5±0.5	17.99±0.12(18.13)
PTB7-Th:IEICO-4F	As Cast	22.87±0.22	0.729±0.002	62.0±0.9	10.34±0.25(10.57)
	CN (265 wt%)	23.70±0.50	0.703±0.002	65.8±1.2	10.95±0.16(11.10)
	DIB (200 wt%)	23.75±0.20	0.725±0.002	66.2±1.6	11.40±0.31(11.81)
P3:Y6	As Cast	24.58±0.20	0.827±0.004	62.9±0.8	12.79±0.14(12.98)
	DIO (110 wt%)	25.45±0.29	0.804±0.008	68.1±2.3	13.88±0.40(14.38)
	DIB (200 wt%)	25.79±0.24	0.805±0.004	70.7±1.1	14.71±0.26(15.12)

a) As cast: without any treatment; CN or DIO: with solvent additive and followed by thermal annealing at 100 °C for 10 min; DIB: with solid additive and followed by MeOH washing. b) Average values were obtained from 5 independent devices and the values in parentheses represent the highest PCEs. All the devices were measured with a mask (aperture area = 3.15 mm^2).

1h, the as-cast and CN-processed devices maintain 80% of their initial efficiencies after being continuously illuminated for 62 and 46 h, respectively, whereas the DIB-processed OSC degraded to 80% of its initial PCE after 72 h of illumination. The results indicate that DIB solid additive can not only improve the PCEs, but also enhance the long-term stability and photostability of OSCs, indicating its great potential in the future manufacturing of OSCs.

Hole and electron mobility of the devices were acquired by using the space-charge-limited current (SCLC) method. As shown in Figure S8, three regions are discriminated from the *J*-*V* curves under the double logarithmic scale. At high voltages (V>1 V), the current shows a quadratic voltage dependence, which typically refers to the SCLC region. For the as-cast PM6:Y6 film, the hole mobility (μ_h) and electron mobility (μ_e) were calculated to be 4.83×10^{-4} and 4.58×10^{-4} cm^2 V^{-1} s^{-1}, respectively. With CN additive, μ_h and μ_e were slightly increased to 5.64×10^{-4} and 5.09×10^{-4} cm^2 V^{-1} s^{-1}, respectively, with a μ_h/μ_e ratio of 1.11. Regarding the devices with DIB additive, μ_h and μ_e were simultaneously promoted to 6.54×10^{-4} and 6.14×10^{-4} cm^2 V^{-1} s^{-1}, respectively, with a μ_h/μ_e ratio of 1.07. The higher and more balanced carrier contributes to the improved J_{sc} and PCE achieved in DIB-processed OSCs.

The morphology of DIB was characterized by using an optical microscope. The DIB film with a thickness of ~100 nm was spin-cast on the PEDOT:PSS/ITO substrate. As shown in Figure 2, DIB film presents lots of aggregates on a length scale of hundred micrometers. We monitored the surface morphology changes of DIB in PM6:Y6 layers (Figure 2a and Figure S9). When 100 wt% DIB is incorporated into PM6:Y6 blend, some rod-like clusters appear on the surface. Further increasing the DIB content to 200 wt %, the rod-like clusters grow into a mass of dendrite-like (blue) and flower-like (yellow) crystals. When the DIB content reaches 300 wt%, dendrite-like and flower-like clusters disappear, and lots of large aggregates cover the entire surface. Intriguingly, after being washed by MeOH, almost all the DIB aggregates disappear, indicating that DIB can be removed by the washing procedure (Figure 2a, right image).

FTIR was used to prove the absence of DIB in the active layer after MeOH washing. As illustrated in Figure 2b, DIB exhibits six strong characteristic peaks at 1,458, 1,372, 1,068, 990, 800, and 460 cm^{-1}, respectively. Fingerprint region (<1,000 cm^{-1}) is useful in distinguishing one molecule from another that contains a functional group. The characteristic peak at 800 cm^{-1} is from the para-substitution of the benzene ring, whereas a characteristic peak at 460 cm^{-1} originates from C–I groups. When 200 wt% DIB was added into PM6:Y6 blend (green line), the characteristic peaks of DIB were clearly seen. After MeOH soaking, the signature peaks related to the para-substitution of the benzene ring and C–I groups disappeared, also verifying the fact that the DIB solid additive was washed away by the MeOH.

X-ray fluorescence (XRF) spectroscopy measurements as a reliable source were also used to evaluate the elemental distributions in BHJ. XRF is highly sensitive to heavy atoms and shows little response for light atoms (atomic number < 20). Organic materials used in this work have no interference to the observation of Iodine (atomic number of 53). As presented in Figure 2c, neat DIB film on silicon substrate

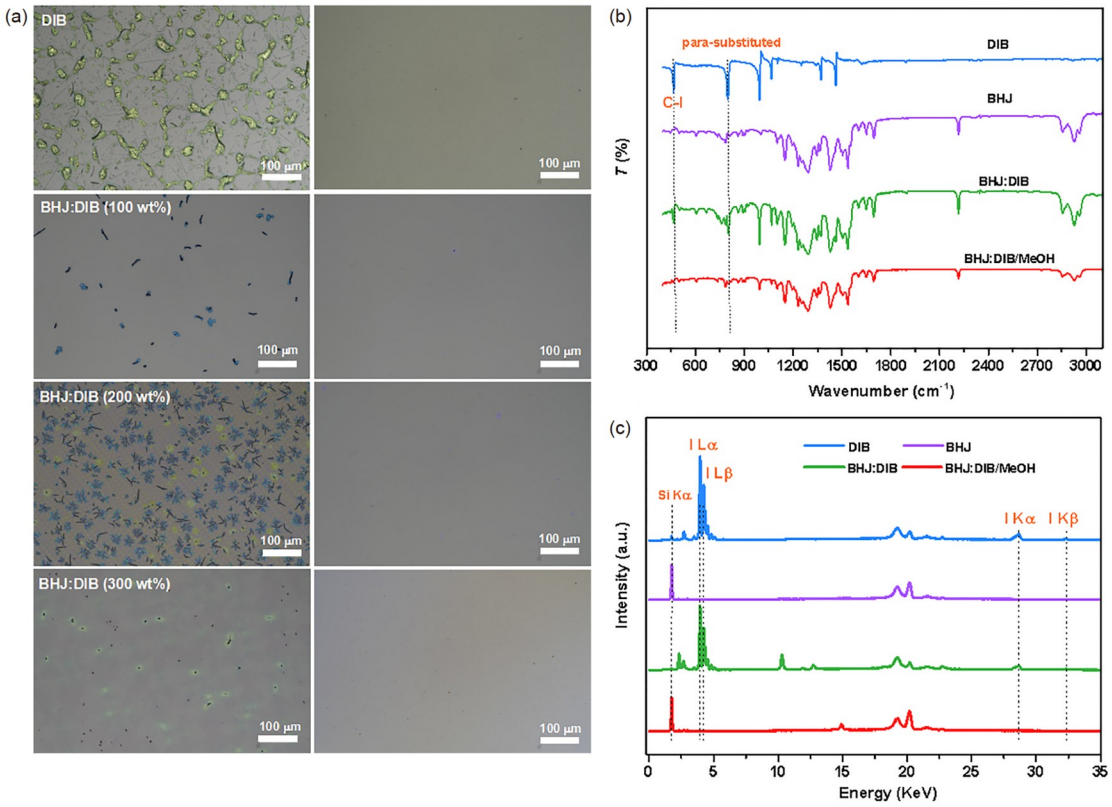

Figure 2 (a) (left) Optical microscope characterizations of neat DIB film and PM6:Y6 films with 100 wt%, 200 wt%, and 300 wt% DIB (ratios of DIB:Y6); (right) the corresponding OM images after washing by MeOH for 5 s. (b) Fourier transform infrared (FTIR) spectra of DIB, PM6:Y6 BHJ and their blend films with and without MeOH washing. (c) X-ray fluorescence spectroscopy of DIB, PM6:Y6 BHJ and their blend films with and without MeOH washing (color online).

shows strong peaks of Kα (28.60 keV), Kβ (32.30 keV), Lα (3.94 keV), and Lβ (4.22), which originate from iodine atoms. As expected, after incorporating 200 wt% DIB into PM6:Y6, the four characteristic peaks from the iodine atom were monitored, and the peaks disappeared after washing by MeOH. It should be noted here that all the samples possess the Si signature at 1.72 eV (Si Kα), indicating the fact that X-ray can go through the whole film. To this end, we can conclude that DIB can be easily removed from the active layer.

Transmission electron microscopy (TEM) was carried out to reveal the influence of DIB solid additive on the active layer morphology. TEM images of the neat and blended films with different DIB contents are shown in Figure 3. For the neat PM6 film processed with DIB (Figure 3a), the fibril network morphology becomes more evident with increasing DIB contents from 0 to 300 wt%, implying that the molecular packing of PM6 was influenced by the DIB contents. Figure 3b shows the TEM images of Y6 film with varying DIB contents. The as-cast Y6 film shows large domain sizes of ~100 nm. The addition of 100 wt% DIB into Y6 has not influenced the domain sizes largely, but further increasing DIB content to 200 wt% induces a higher degree of aggregation of Y6 and forms crystalline domains. The continuously increasing DIB content to 300 wt% results in a more serious aggregation of Y6. TEM results indicate that DIB solid additive not only enables the polymer donors to self-assemble into clearer fibril structures but also induces Y6's aggregation. This viewpoint has been further verified in the blend morphology. As shown in Figure 3c, large-scale aggregation was observed in the as-cast PM6:Y6 blend. A fibrillar network morphology with appropriate phase separation was achieved in PM6:Y6 blend with 200 wt% DIB. The morphology of the films using CN solvent additive was also studied as shown in Figures S10, S11. Compared with the CN-treated blend, DIB-processed blend exhibited an optimized fibril network and better phase separation, which is more beneficial for excitation dissociation and charge transport [18].

The molecular orientation and packing behavior of PM6 and Y6 with DIB additives were investigated by GIWAXS. 2D GIWAXS patterns and the corresponding line cuts are shown in Figure 4. For the as-cast PM6 films (Figure 4a, b), the major lamellar diffraction peaks at q = 0.3 and 0.9 Å^{-1}, and a strong π-π diffraction peak at q = 1.67 Å^{-1} were observed in the out-of-plane (OOP) direction. The crystal co-

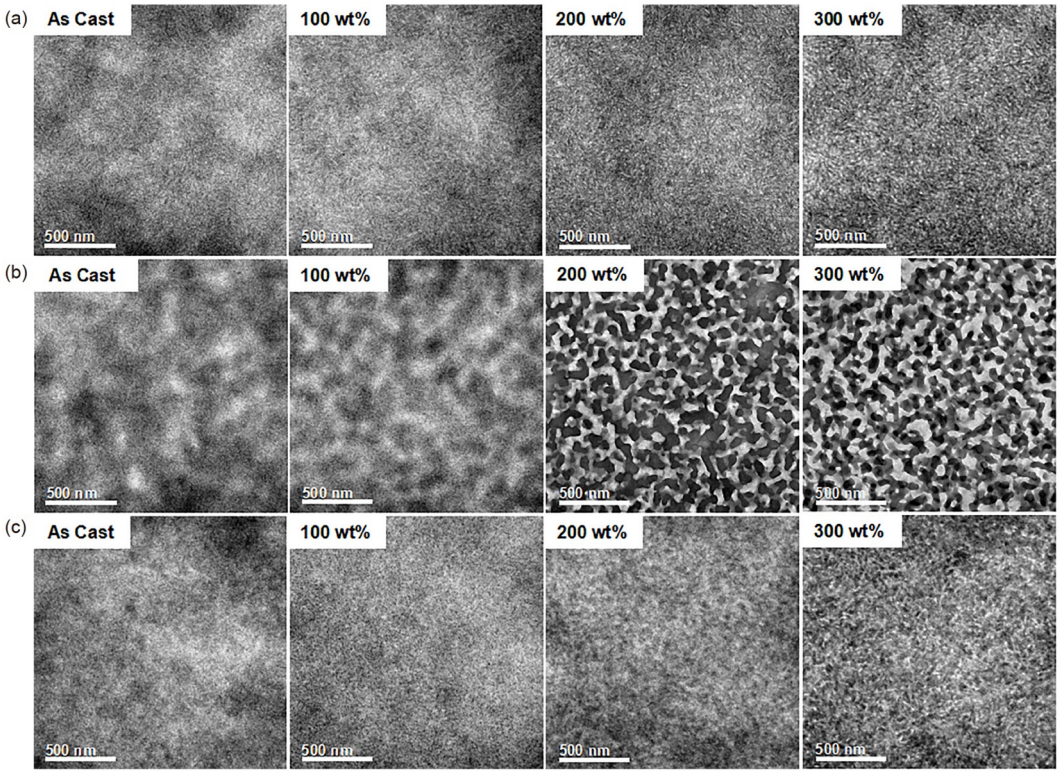

Figure 3 Influence of solid additives on blend morphology. TEM images of (a) PM6, (b) Y6, and (c) PM6:Y6 films processed with 0, 100 wt%, 200 wt%, and 300 wt% DIB.

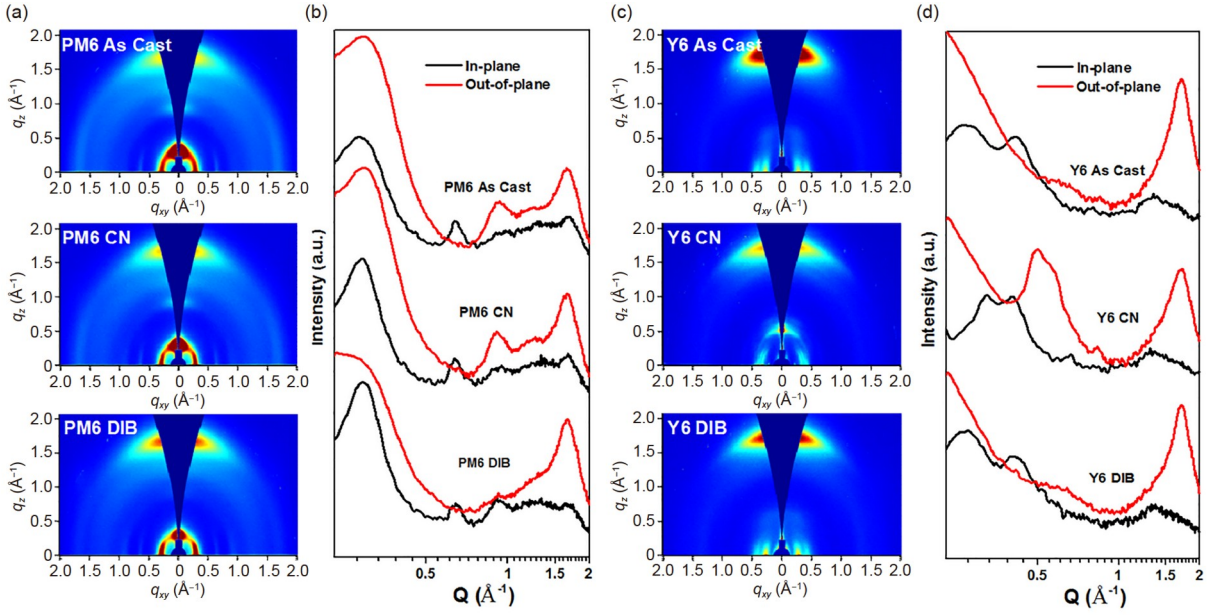

Figure 4 (a) 2D GIWAXS diffraction patterns of PM6 films processed with different methods and (b) the corresponding 1D line-cut profiles. (c) 2D GIWAXS diffraction patterns of Y6 films processed with different methods and (d) the corresponding 1D line-cut profiles (color online).

herence length (CCL) of the (010) π-π diffraction peak in the OOP direction was calculated to be 20.7 Å (Table S2). These results indicate that PM6 has a semi-crystalline structure with a mixed face-on and edge-on orientation. Compared with the as-cast PM6, PM6 films processed with CN solvent additive showed the increased intensity of diffraction peak at q_z = 1.67 Å^{-1} in the OOP direction with a CCL value of 23.7 Å, indicating that the crystalline packing of PM6 is

improved by the CN treatment. Regarding the PM6 film treated with 200 wt% DIB, the scattering intensity of π-π stacking in the OOP direction was further intensified with a higher CCL value of 26.0 Å when compared with the as-cast and CN-treated PM6 films. Meanwhile, the intensity of lamellar diffraction peak at q_z = 0.3 Å^{-1} in the OOP direction was decreased. These results suggest that PM6 adopts a preferential face-on orientation and improves crystallinity with the treatment of DIB. Different from the trend of as-cast PM6 and DIB-processed films, the CN treatment decreased the π-π stacking of Y6, evidenced by the weaker π-π diffraction peak at q_z = 1.70 Å^{-1} in the OOP direction with a smaller CCL value (25.8 Å). In contrast, DIB was found to slightly increase the Y6 packing with a relatively large CCL value of 32.9 Å in comparison with the as-cast film (CCL = 32.0 Å). The GIWAXS profiles of PM6:Y6 blends with and without processing additives (CN and DIB) are shown in Figure S12. A strong π-π diffraction peak at q_z = 1.70 Å^{-1} in the OOP direction was found for all the blend films, indicative of the preferential face-on orientation of PM6:Y6. In detail, the CN- and DIB-treated blends improved crystalline packing with the larger CCLs (~29.0 Å) than that (26.7 Å) of the as-cast blend. The GIWAXS results suggest that DIB can simultaneously improve the crystalline ordering of both PM6 and Y6, showing a good agreement with the morphology observed in the TEM results.

Theoretical calculations were also carried out to explore the non-covalent interactions of DIB/PM6 and DIB/Y6 at the B3LYP/6-31G(d,p)/LanL2DZ level (Figure 5**)**. The calculated results indicate negative binding energies of DIB with PM6 and Y6 with quite similar values. Different non-covalent interactions were involved in the DIB/PM6 and DIB/Y6 structures. In the DIB/Y6 structure with a binding energy of −2.9 kcal/mol, there are C–H···N and C–H···I hydrogen bond interactions, whereas a C–H···O hydrogen bond interaction in the DIB/PM6 structure with a binding energy of −2.2 kcal/mol was observed. It seems that the presence of hydrogen bonds between PM6 or Y6 molecules enhances their interactions. Since the binding energies of DIB with PM6 and Y6 are moderate, the DIB can be easily washed away by the MeOH. Combined with the experiment results and theoretical calculations, the possible working mechanism of DIB is proposed. During the spin-coating process, DIB can easily grow into microcrystals. Due to the presence of weak non-covalent interactions, including C–H···O/C–H···N hydrogen bond interaction and C–H···I hydrogen bond interaction, in DIB:PM6 and DIB:Y6 structure, the crystallization and aggregation of PM6 (or Y6) are improved. By controlling the DIB content, the degree of crystallization and aggregation of the active layer can be fine-tuned, and thereby yields an optimal bicontinuous network morphology. Finally, DIB can be removed due to its solubility in MeOH and the moderate binding energies of DIB/PM6 and DIB/Y6.

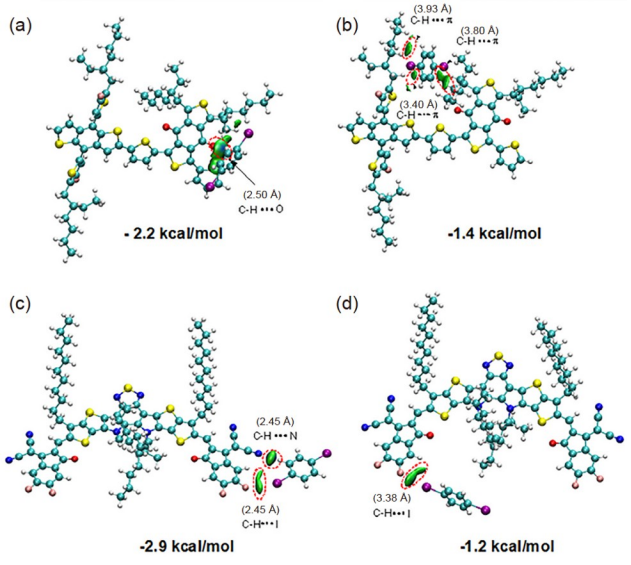

Figure 5 (a, b) Optimized PM6-DIB complex structures, hydrogen bond length, and the corresponding binding energy. (c, d) Optimized Y6-DIB complex structures, hydrogen bond length, and the corresponding binding energy (color online).

3 Conclusions

In conclusion, we report an alcohol washable solid additive, which improves the active layer morphology, photovoltaic performance, and stability of NFA-OSCs. The solid additive shows non-covalent coulombic interaction (*e.g.*, hydrogen bond) with both donor and acceptor, which can improve the polymer crystalline packing and facilitate the non-fullerene acceptor aggregation. Thus, the morphology of the active layer is finely controlled by the treatment of DIB with varying its concentration. Most importantly, DIB can be easily removed from the active layer *via* a simple alcohol washing process (without thermal annealing treatment), which is appealing for large-scale manufacturing of OSCs. As a result, the OSCs based on PM6:Y6 achieve a PCE of 17.47%, outperforming the as-cast (16.46%) and CN-treated (17.02%) OSCs. We also showed its general applicability in different donor/acceptor systems. Among them, PM6:BTP-eC9 OSCs affords an impressively high FF of 79.8% and outstanding PCE of 18.13% (certified as 17.7%), which is among the highest efficiencies in binary OSCs to date. In addition, the OSCs processed with DIB solid additive exhibits excellent long-term storage stability and photostability. Before the submission of our work, we noticed that similar work was published [40], in which DIB was also utilized as a solid additive in non-fullerene OSCs and a TA treatment is needed to remove the residue of DIB in the blend film. Our work demonstrates that alcohol-washable solid additive is a promising strategy for the fabrication of high-

performance and stable OSCs.

Acknowledgements This work was supported by the National Natural Science Foundation of China (52003013, 21734001, 51825301) and China Postdoctoral Science Foundation (BX20190023). H. W. Y acknowledges the financial support by the National Research Foundation (NRF) of Korea (2016M1A2A2940911, 2019R1A6A1A11044070). The authors thank Prof. Yanlin Song (ICCAS) for the assistance with optical microscope measurements.

Conflict of interest The authors declare no conflict of interest.

Supporting information The supporting information is available online at http://chem.scichina.com and http://link.springer.com/journal/11426. The supporting materials are published as submitted, without typesetting or editing. The responsibility for scientific accuracy and content remains entirely with the authors.

1 Yan C, Barlow S, Wang Z, Yan H, Jen AKY, Marder SR, Zhan X. *Nat Rev Mater*, 2018, 3: 18003
2 Cheng P, Li G, Zhan X, Yang Y. *Nat Photon*, 2018, 12: 131–142
3 Lin Y, Wang J, Zhang ZG, Bai H, Li Y, Zhu D, Zhan X. *Adv Mater*, 2015, 27: 1170–1174
4 Zhao W, Li S, Yao H, Zhang S, Zhang Y, Yang B, Hou J. *J Am Chem Soc*, 2017, 139: 7148–7151
5 Yuan J, Zhang Y, Zhou L, Zhang G, Yip HL, Lau TK, Lu X, Zhu C, Peng H, Johnson PA, Leclerc M, Cao Y, Ulanski J, Li Y, Zou Y. *Joule*, 2019, 3: 1140–1151
6 Liu Q, Jiang Y, Jin K, Qin J, Xu J, Li W, Xiong J, Liu J, Xiao Z, Sun K, Yang S, Zhang X, Ding L. *Sci Bull*, 2020, 65: 272–275
7 Cui Y, Yao H, Zhang J, Xian K, Zhang T, Hong L, Wang Y, Xu Y, Ma K, An C, He C, Wei Z, Gao F, Hou J. *Adv Mater*, 2020, 32: 1908205
8 Zhang M, Zhu L, Zhou G, Hao T, Qiu C, Zhao Z, Hu Q, Larson BW, Zhu H, Ma Z, Tang Z, Feng W, Zhang Y, Russell TP, Liu F. *Nat Commun*, 2021, 12: 309
9 Li C, Zhou J, Song J, Xu J, Zhang H, Zhang X, Guo J, Zhu L, Wei D, Han G, Min J, Zhang Y, Xie Z, Yi Y, Yan H, Gao F, Liu F, Sun Y. *Nat Energy*, 2021, 6: 605–613
10 Lin Y, Firdaus Y, Isikgor FH, Nugraha MI, Yengel E, Harrison GT, Hallani R, El-Labban A, Faber H, Ma C, Zheng X, Subbiah A, Howells CT, Bakr OM, McCulloch I, Wolf SD, Tsetseris L, Anthopoulos TD. *ACS Energy Lett*, 2020, 5: 2935–2944
11 Jørgensen M, Norrman K, Gevorgyan SA, Tromholt T, Andreasen B, Krebs FC. *Adv Mater*, 2012, 24: 580–612
12 Guo J, Min J. *Adv Energy Mater*, 2018, 9: 1802521
13 Zhang Y, Samuel IDW, Wang T, Lidzey DG. *Adv Sci*, 2018, 5: 1800434
14 Baran D, Ashraf RS, Hanifi DA, Abdelsamie M, Gasparini N, Röhr JA, Holliday S, Wadsworth A, Lockett S, Neophytou M, Emmott CJM, Nelson J, Brabec CJ, Amassian A, Salleo A, Kirchartz T, Durrant JR, McCulloch I. *Nat Mater*, 2017, 16: 363–369
15 Xue R, Zhang J, Li Y, Li Y. *Small*, 2018, 14: 1801793
16 Zhao F, Wang C, Zhan X. *Adv Energy Mater*, 2018, 8: 1703147
17 Gurney RS, Lidzey DG, Wang T. *Rep Prog Phys*, 2019, 82: 036601
18 Xia T, Cai Y, Fu H, Sun Y. *Sci China Chem*, 2019, 62: 662–668
19 Liu T, Huo L, Chandrabose S, Chen K, Han G, Qi F, Meng X, Xie D, Ma W, Yi Y, Hodgkiss JM, Liu F, Wang J, Yang C, Sun Y. *Adv Mater*, 2018, 30: 1707353
20 Xie Y, Yang F, Li Y, Uddin MA, Bi P, Fan B, Cai Y, Hao X, Woo HY, Li W, Liu F, Sun Y. *Adv Mater*, 2018, 30: 1803045
21 Jiao X, Ye L, Ade H. *Adv Energy Mater*, 2017, 7: 1700084
22 McDowell C, Abdelsamie M, Toney MF, Bazan GC. *Adv Mater*, 2018, 30: 1707114
23 Manley EF, Strzalka J, Fauvell TJ, Marks TJ, Chen LX. *Adv Energy Mater*, 2018, 8: 1800611
24 van Franeker JJ, Turbiez M, Li W, Wienk MM, Janssen RAJ. *Nat Commun*, 2015, 6: 6229
25 Kim Y, Yeom HR, Kim JY, Yang C. *Energy Environ Sci*, 2013, 6: 1909–1916
26 Zhao J, Li Y, Yang G, Jiang K, Lin H, Ade H, Ma W, Yan H. *Nat Energy*, 2016, 1: 15027
27 Su MS, Kuo CY, Yuan MC, Jeng US, Su CJ, Wei KH. *Adv Mater*, 2011, 23: 3315–3319
28 Liao HC, Ho CC, Chang CY, Jao MH, Darling SB, Su WF. *Mater Today*, 2013, 16: 326–336
29 Tremolet de Villers BJ, O'Hara KA, Ostrowski DP, Biddle PH, Shaheen SE, Chabinyc ML, Olson DC, Kopidakis N. *Chem Mater*, 2016, 28: 876–884
30 Xie Y, Hu X, Yin J, Zhang L, Meng X, Xu G, Ai Q, Zhou W, Chen Y. *ACS Appl Mater Interfaces*, 2017, 9: 9918–9925
31 Cheng P, Zhan X. *Chem Soc Rev*, 2016, 45: 2544–2582
32 Lee S, Kong J, Lee K. *Adv Energy Mater*, 2016, 6: 1600970
33 Yu R, Yao H, Hong L, Qin Y, Zhu J, Cui Y, Li S, Hou J. *Nat Commun*, 2018, 9: 4645
34 Ye L, Cai Y, Li C, Zhu L, Xu J, Weng K, Zhang K, Huang M, Zeng M, Li T, Zhou E, Tan S, Hao X, Yi Y, Liu F, Wang Z, Zhan X, Sun Y. *Energy Environ Sci*, 2020, 13: 5117–5125
35 Zhu L, Zhang M, Zhou G, Hao T, Xu J, Wang J, Qiu C, Prine N, Ali J, Feng W, Gu X, Ma Z, Tang Z, Zhu H, Ying L, Zhang Y, Liu F. *Adv Energy Mater*, 2020, 10: 1904234
36 Gao K, Deng W, Xiao L, Hu Q, Kan Y, Chen X, Wang C, Huang F, Peng J, Wu H, Peng X, Cao Y, Russell TP, Liu F. *Nano Energy*, 2016, 30: 639–648
37 Lv J, Tang H, Huang J, Yan C, Liu K, Yang Q, Hu D, Singh R, Lee J, Lu S, Li G, Kan Z. *Energy Environ Sci*, 2021, 14: 3044–3052
38 Fu J, Chen S, Yang K, Jung S, Lv J, Lan L, Chen H, Hu D, Yang Q, Duan T, Kan Z, Yang C, Sun K, Lu S, Xiao Z, Li Y. *iScience*, 2020, 23: 100965
39 Zhang Y, Cho Y, Lee J, Oh J, Kang SH, Lee SM, Lee B, Zhong L, Huang B, Lee S, Lee JW, Kim BJ, Li Y, Yang C. *J Mater Chem A*, 2020, 8: 13049–13058
40 Fu J, Chen H, Huang P, Yu Q, Tang H, Chen S, Jung S, Sun K, Yang C, Lu S, Kan Z, Xiao Z, Li G. *Nano Energy*, 2021, 84: 105862
41 Min J, Kwon OK, Cui C, Park JH, Wu Y, Park SY, Li Y, Brabec CJ. *J Mater Chem A*, 2016, 4: 14234–14240